THE ASTROPHYSICAL JOURNAL, 400:535–550, 1992 December 1

SUBMILLIMETER LINE OBSERVATIONS OF THE PROTO–PLANETARY NEBULA CRL 2688

P. A. JAMINET[1] AND W. C. DANCHI
Department of Physics and Space Sciences Laboratory, University of California, Berkeley, CA 94720

GÖRAN SANDELL
Joint Astronomy Centre, 665 Komohana St., Hilo, HI 96720

AND

E. C. SUTTON[2]
Department of Astronomy, University of Illinois, 1002 W. Green Street, Urbana, IL 61801
Received 1991 October 11; accepted 1992 June 4

ABSTRACT

We have observed the proto–planetary nebula CRL 2688 with 14″ resolution in the following submillimeter-wavelength lines: CO $J = 3$–2, ^{13}CO $J = 3$–2, C^{17}O $J = 3$–2, CS $J = 7$–6, HCN $J = 4$–3, H^{13}CN $J = 4$–3, CN $N = 3$–2, HC_3N $J = 38$–37 and $J = 39$–38, and HN^{13}C $J = 4$–3. We mapped the envelope in CO, ^{13}CO, CS, and H^{13}CN. The submillimeter lines show strong emission from two components of the envelope: a cold, dense, optically thick slow wind and a warm, optically thin fast wind. In our maps, the slow wind appears compact and circularly symmetric. The fast wind is somewhat extended and asymmetric; it appears to have two bipolar components, one along the N–S axis in which blueshifted emission is to the north and redshifted emission to the south, the other along the E–W axis in which blueshifted emission is to the east and redshifted emission to the west. We estimate a mass-loss rate in the fast wind of about $2 \times 10^{-5}\ M_\odot\ \mathrm{yr}^{-1}$, if the wind was continuous. The ^{12}C:^{13}C ratio in the fast wind is 5, compared to about 20 in the slow wind. The value in the fast wind is equal to the CN-cycle equilibrium ratio and suggests that envelope burning has occurred. The HCN:CO abundance ratio may be lower in the fast wind than in the slow wind.

The CO $J = 3$–2 and HCN $J = 4$–3 lines are brighter than is consistent with the model of Truong-Bach et al. The discrepancy may be due to emission from fast wind material at projected velocities near line center. It is clear that the kinetic temperature falls rapidly with radius, accounting for the compact nature of emission from the dense slow wind. Despite the compactness of the emission, we observed variations with position in the velocity centroid of the line profiles. These variations were similar to those observed in HCN $J = 1$–0 by Bieging & Nguyen-Q-Rieu, which they attributed to rotation of the envelope. We believe that the velocity gradients are not caused by rotation, but rather by asymmetries in the envelope associated with the fast wind.

Subject headings: ISM: kinematics and dynamics — ISM: molecules — planetary nebulae: individual (CRL 2688)

1. INTRODUCTION

The transitional (proto–planetary nebula, or PPN) stage between the asymptotic giant branch (AGB) and the formation of a planetary nebula (PN) may be, next to the period of star formation, the least understood phase in the life of an intermediate-mass star. Study of the PPN phase has been hampered by the relatively small number of these objects. Most PPN candidates lie at large distances and therefore envelopes are hard to resolve or observe in detail. In addition, obscuration by their massive envelopes can prevent direct observation of the central stars and make it difficult to distinguish PPN and AGB stars. Currently the leading PPN candidates fall among the class of bipolar nebulae. The optically bright F or G type giants with large infrared excesses are probably bipolar nebulae seen face-on (Hrivnak & Kwok 1991; van der Veen, Habing, & Geballe 1989).

Bipolar nebulae differ from most AGB stars in many respects. Most AGB stars appear to lose mass with approximate spherical symmetry, whereas bipolar nebulae seem to have large mass-loss rates along an equatorial plane and relatively small mass-loss rates along a polar axis. Mass-loss rates in the bipolar nebulae are much higher than in AGB stars, and unlike AGB stars the mass loss is super-Eddington, in the sense that momentum in the winds exceeds the momentum in radiation (Knapp 1986). While AGB stars generally have slow winds with expansion velocities typically about 15–20 km s^{-1}, bipolar nebulae exhibit both slow and fast molecular winds. The fast winds typically have expansion velocities of 50–200 km s^{-1} (e.g., Kawabe et al. 1987; Morris et al. 1987; Gammie et al. 1989). The bipolar nebula stage appears to begin before the star evolves off the AGB. The central giant of the bipolar nebula OH 231.8+4.2, for instance, has a spectral classification consistent with a late AGB star (Cohen 1981), and in other bipolar nebulae the development of asphericity in the mass loss predated the evolution of the central star off the AGB. However, with the exception of OH 231.8+4.2 the central stars of known bipolar nebulae are warmer than AGB stars (e.g., Crampton, Cowley, & Humphreys 1975 and Westbrook et al. 1975), indicating that the bipolar phase of the AGB is not long compared to the PPN lifetime, which is itself typically only a few thousand years.

It is not entirely clear whether all PPN or only some share the bipolar symmetry pattern of a dense equatorial plane and a

[1] Current postal address: Harvard-Smithsonian Center for Astrophysics, 60 Garden Street, Cambridge, MA 02138.

[2] Also Department of Electrical & Computer Engineering, University of Illinois, and Department of Physics and Space Sciences Laboratory, University of California at Berkeley.

more tenuous polar axis. Most PNs possess approximate bipolar symmetry (Zuckerman & Aller 1986), and models with bipolar symmetry have been successful in explaining a wide variety of observed PN shapes (Masson 1990; Icke, Balick, & Frank 1992). Even the youngest PNs show bipolar structure (Aaquist & Kwok 1991), and in the one PN in which both the ionized gas and its surrounding molecular envelope have been studied in detail, NGC 7027, it is clear that bipolarity developed long before the formation of the PN (Jaminet et al. 1991). These observations and models of PNs suggest that the PPN phase of all or most stars, not just binary stars, is bipolar.

A controversial issue is whether the bipolar symmetry pattern is caused by the gravitational influence of a binary companion or by centrifugal forces due to rotation of the central star; both forces are weak. Morris (1981), for instance, has suggested that bipolar nebulae represent the late AGB or PPN stage of binary stars. There are indications of binary systems in several bipolar nebulae. Morris & Reipurth (1990) have suggested that the apparent oscillation of the bipolar symmetry axis in IRAS 09371+1212, the Frosty Leo nebula, may be due to precession of the central giant. OH 231.8+4.2 may have a blue companion to its central M-type giant (Cohen et al. 1985). However, most bipolar nebulae are not known to be binary systems. The fact that even PNs not usually classed as bipolar—NGC 7027, for instance—share the bipolar symmetry pattern suggests that the differences between bipolar and nonbipolar nebulae are one of degree, not of kind.

There is evidence that the bipolar nebulae arise from high-mass progenitors, while spherical nebulae arise from low-mass progenitors. It has long been known (Greig 1972) that the bipolar PNs (Greig's class B) lie in circular orbits in the galactic plane, characteristic of Population I or younger, higher mass stars, while many of the spherical nebulae (Greig's class C) lie in the halo and presumably derive from Population II, lower mass stars. Moreover, bipolar PNs tend to have high N/O ratios, indicating that they were massive enough to undergo envelope burning, while spherical nebulae have low N/O ratios characteristic of lower mass progenitors (Kaler 1983). Because higher mass progenitors rotate faster, one would expect this correlation between progenitor mass and bipolarity if rotation causes the bipolarity. If binary companions cause bipolarity, it is not obvious that progenitor mass should correlate so well with bipolarity.

Among the nearest, and best studied, of the bipolar nebulae is CRL 2688, also known as the Egg nebula for its location beneath the hindquarters of the Cygnus Swan. The central star has an effective temperature of 8000 K (Crampton et al. 1975; Cohen & Kuhi 1977). CRL 2688 may have been on the AGB, with an effective temperature less than 3000 K, as little as 200 yr ago (Jura & Kroto 1990). In the optical and infrared CRL 2688 appears strongly bipolar (Ney et al. 1975), and the axially symmetric model of Yusef-Zadeh, Morris, & White (1984) successfully accounted for the optical nebulosity. However, in molecular line emission the nebula appears more complex. Bieging & Nguyen-Q-Rieu (1988, hereafter BNQR) found that the velocity centroid of HCN $J = 1$–0 emission from CRL 2688 varied, not only along the N–S symmetry axis of the Yusef-Zadeh et al. model, but also along the orthogonal E–W axis. If the envelope is in fact axially symmetric, this variation implies rotation of the envelope, with huge angular momentum. Smith et al. (1990) found that emission from the $S(1)$ line of molecular hydrogen occurs in four lobes, with two blue-shifted lobes located north and east of nebula center and two redshifted lobes located south and west of nebula center. This velocity distribution resembles the HCN velocity distribution found by BNQR. However, the H_2 $S(1)$ velocity distribution could not have been caused by envelope rotation, and it is not clear how the H_2 $S(1)$ morphology can be reconciled with the bipolarity of the optical nebulosity.

Submillimeter observations, for the most part, observe excited lines from molecules which have ground-state lines at millimeter wavelengths. Therefore, submillimeter observations are helpful in understanding the excitation and abundances of molecules observed at millimeter wavelengths. But submillimeter observations are especially valuable in the case of PPN. Because spontaneous emission rates rise rapidly with frequency, the submillimeter lines can be considerably brighter than millimeter lines in warm, optically thin gas. Thus the submillimeter is the frequency region of choice for observing emission from the fast winds of PPN, which tend to be optically thin and arise in warm, excited gas. These fast winds are especially interesting because neither their morphology, nor their mass-loss rates, nor their elemental and chemical abundances, have yet been determined with confidence in any PPN.

2. OBSERVATIONS

The observations were made during 1990 March, at the 15 m James Clerk Maxwell Telescope, located on Mauna Kea, Hawaii, using the 345 GHz SIS receiver constructed at the University of California at Berkeley (Sutton et al. 1990). The observations were performed using a beam-switching mode, with chopping between on-source and off-source positions at 1 Hz. Off-source positions were typically offset 2′ in azimuth from the on-source position. This technique generally gave quite flat spectra with a consistent continuum level, except at the very edges of the bandpass where roll-off in the response of the AOS contributed to poor baseline subtraction. We have in all cases subtracted the level of the continuum emission from the spectra. In a few cases in which baseline errors were introduced (these errors are easily detected because the baseline acquires the shape of the receiver/AOS IF gain profile), we have subtracted a linear fit to the apparent continuum from the region of the spectral line. Baseline fluctuations, which are caused by inexact subtraction of the atmospheric emission, were typically about 0.1 K peak to trough within the central 400 MHz of our IF band.

Calibration was obtained by the chopper-wheel method in which intensities are scaled by dividing the difference between spectra of the source and the sky by the difference between spectra of a blackbody at ambient temperature and the sky. Because CRL 2688 has a size comparable to our main beam, we present our data in units of main beam brightness temperature. A main beam efficiency of 0.54 was derived from observations of Venus, Jupiter, and Saturn, and an extended source efficiency of 0.72 was derived from observations of the Moon. Beam maps were made on Mars and show a circularly symmetric, Gaussian beam with a full width at half-maximum of 13″.7 at the ^{12}CO $J = 3$–2 frequency. We estimate calibration uncertainties of about 20% for CO $J = 3$–2, CS $J = 7$–6 and HC_3N $J = 38$–37; of 30% for most other lines; and of 40% for ^{13}CO $J = 3$–2, which is subject to large and unbalanced (between the sidebands) atmospheric attenuation and lies at a frequency for which the receiver sideband balance is less certain than at other frequencies.

Although the whether was excellent during these observations, pointing was a concern. CRL 2688 rises during March

only slightly earlier than the Sun, and many of these observations were performed after dawn. The atmosphere was generally quite stable during this period, but the warming of the dish after sunrise affected the pointing. We checked the pointing every 15 minutes after dawn, but even with such frequent adjustments, corrections of as much as 3″–4″ had to be made occasionally. In a compact source such as CRL 2688, 3″–4″ can be significant. In general, the data presented in this paper were acquired during times of stable pointing. Some data not presented here, in particular our map in the ^{13}CO $J = 3$–2 line, were acquired during periods of unstable pointing.

We adopted a central position for CRL 2688 of $\alpha(1950) = 21^h00^m19^s.9$, $\delta(1950) = +36°29'45''$. In the maps, we used square grids with spacings of 7″ in right ascension and declination, except in the case of $H^{13}CN$ $J = 4$–3, in which we used a grid spacing of 6″.

3. DATA AND ANALYSIS

We present in § 3.1 spectra toward the central position in each of the lines we observed, and our interpretation of each line in terms of its opacity and the excitation and abundance of the species involved; in § 3.2, we present our maps. We have performed detailed statistical equilibrium calulations and modeling for CO and its isotopic variants; for other molecules the grounds for our interpretations of line opacities and molecular excitation and abundances are described in the text. Our CO model is similar to that described in the appendix to Jaminet et al. (1991), but vibrationally excited levels are included.

In the discussion which follows it is important to treat emission from the fast and slow winds separately. This division is necessary because the slow and fast winds in CRL 2688 have, as we will show, radically different excitation conditions and differences in some molecular abundances. However, the division is also somewhat artificial, because in these observations we cannot completely distinguish between slow and fast wind emission. Emission from fast wind material can appear at the same projected velocities as emission from slow wind material, a fact which must be kept in mind when discussing emission near line center. In many lines emission from slow wind material dominates over emission from fast wind material near line center, but this is not always true. And when subtle changes in line profiles are discussed, as in § 3.2, it should be remembered that both fast wind emission and slow wind emission may contribute to the observed variations.

3.1. *Spectra*

3.1.1. CO, ^{13}CO, *and* $C^{17}O$

The brightness of the CO $J = 3$–2 line (Fig. 1*a*) appears to be consistent with the progression in brightness temperatures found in $J = 1$–0 and $J = 2$–1 observations. In observations with similar beam size to ours, Kawabe et al. (1987) found a peak main beam brightness temperature in the $J = 1$–0 line of about 7.5 K in a 15″ beam, while Truong-Bach et al. (1990, hereafter TB90) found a peak $J = 1$–0 brightness of 8 K in a 23″ beam. (The TB90 $J = 1$–0 brightness calls into question the Kawabe et al. calibration, as the emission should be brighter in the smaller beam.) TB90 found a peak temperature in the $J = 2$–1 line of 15 K in a 12″ beam. We find a peak temperature in the $J = 3$–2 line of 16 K in a 14″ beam. The pattern of increased brightness temperature at higher J is evidence for effective thermalization of the CO in all these lines. If the level populations are thermalized then the rapid increase in spontaneous emission rates with J tends to make higher J lines more optically thick, and brighter. However, as we discuss in § 4.3, our observed brightness temperature is not consistent in detail with the model of TB90. TB90 estimate a mass-loss rate ($1.7 \times 10^{-4}\ M_\odot\ yr^{-1}$) and a CO:$H_2$ ratio (6×10^{-4}) that are together sufficient to make the $J = 2$–1 and $J = 3$–2 lines highly optically thick. Under these circumstances our $J = 3$.–2 brightness temperature would be somewhat less than TB90's $J = 2$–1 brightness temperature, partly because of our larger beam and partly because of the less effective excitation of the higher J levels under TB90's temperature distribution. That the reverse is true implies, for a single-component, spherically symmetric model, that the envelope is warmer, and the CO less optically thick, than predicted by TB90. In § 4.3, we speculate that the difference between our observations and the TB90 model predictions may be due, in part, to emission near line center by warm, optically thin material in the fast wind.

In the less optically thick ^{13}CO lines the observed brightness temperatures increase more rapidly with J than in ^{12}CO. The ratio of the line intensities ^{12}CO:^{13}CO is approximately 7–12 in the $J = 1$–0 line Spoka et al. 1989; Bujarrabal et al. 1988, hereafter BGBM), 4.4 in the $J = 2$–1 line (Wannier & Sahai 1987), and 3 in the $J = 3$–2 line (this work; see Fig. 1*b*), showing that the ^{13}CO lines are not optically thick. The ^{12}CO:^{13}CO ratio in the $J = 3$–2 lines varies from about 2 near the line edge to about 3.5 at line center; this pattern indicates that opacities are smallest at line center, as is usually the case in CSE line profiles, and that the ^{13}CO $J = 3$–2 optical depth is on the order of or less than unity at most projected velocities. The ^{13}CO $J = 3$–2 line shows evidence for modest self-absorption at $v_{lsr} = -53$ km s^{-1}, suggesting the existence of a shell with an optical depth of at least several tenths in which the $J = 2$ level is excited but the $J = 3$ level is subthermally populated. This opacity in the self-absorption feature typically indicates a radial line opacity on the order of or somewhat larger than unity. The ^{13}CO $J = 3$–2 line profile has an interesting shape; it is roughly parabolic, like the CO $J = 3$–2 line profile, at velocities more than about 7 km s^{-1} from line center, and has a bowl-shaped dip within 7 km s^{-1} from line center. This pattern suggests optically thin emission at line center. Such patterns are not unusual in CSE's, because radial opacities tend to be much larger than tangential opacities even in aspherical envelopes. Thus line opacity tends to vary substantially with projected radial velocity, having its minimum at line center and maximum at the line edge. The shape of the ^{13}CO $J = 3$–2 line profile suggests that its line opacity passes through $\tau = 1$ at about 7 km s^{-1} from line center.

The $C^{17}O$ $J = 3$–2 line (Fig. 1*c*) is definitely optically thin; its brightness is consistent with that found by Wannier & Sahai (1987) in the $J = 2$–1 line. The ^{13}CO and $C^{17}O$ intensities we observe appear consistent with a ^{12}CO:^{13}CO abundance ratio of 20 and a ^{12}CO:$C^{17}O$ abundance ratio of 300, as estimated by Wannier & Sahai. It should be kept in mind, however, that these isotope ratio estimates are model-dependent, and a satisfactory model for CRL 2688 has not yet been developed.

The CO line wings are optically thin. The brightness temperatures in the CO line wings for the 1–0 line observed at the 45 m Nobeyama Radio Observatory (Kawabe et al. 1987), the 2–1 line observed at the 30 m IRAM telescope (TB90), and the 3–2 line observed at the 15 m JCMT (this work), all with comparable beam sizes, are in proportions of 1:3:5, a progression which is possible only for optically thin emission from warm gas. Moreover, the ratio of intensity at line center to

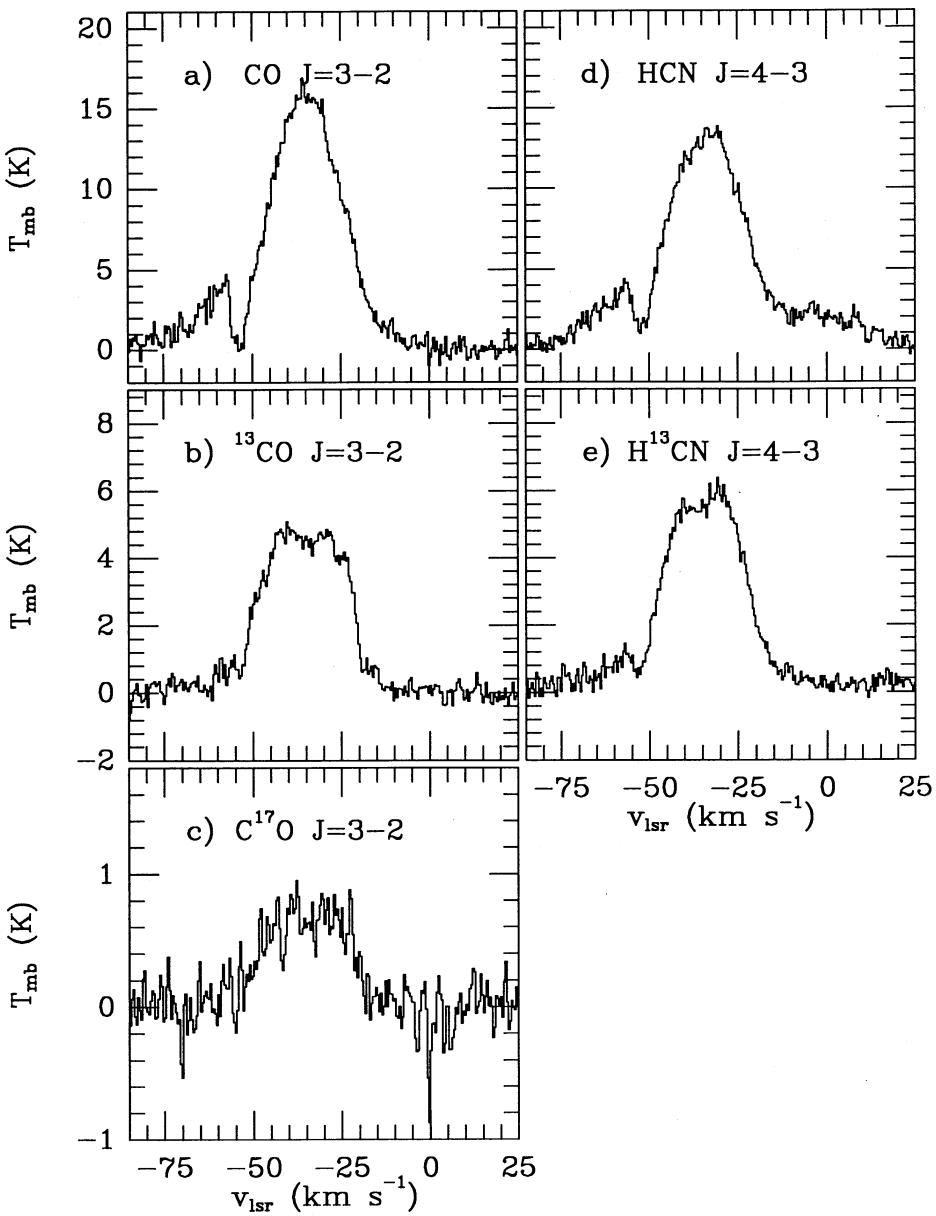

FIG. 1.—Spectra toward the central position of CRL 2688. (*a*) CO $J = 3$–2; (*b*) ^{13}CO $J = 3$–2; (*c*) C^{17}O $J = 3$–2; (*d*) HCN $J = 4$–3; (*e*) H^{13}CN $J = 4$–3.

intensity in the line wings, which is independent of possible calibration errors, also decreases rapidly as J increases, providing further proof that the line wing emission is not optically thick.

Our data include, for the first time, an observation with good signal-to-noise ratio of the line wings in ^{13}CO. We also observe prominent line wings in H^{13}CN (see Fig. 1*e*); Nguyen-Q-Rieu & Bieging (1990; hereafter NQRB) previously observed line wings in this molecule. The line wings are remarkably bright in these two molecules; integrated intensity is one-fifth that in the corresponding CO and HCN line wings. As the line wings are optically thin, we infer that the ^{12}C:^{13}C ratio in the fast wind is 5. This ratio is different from that in the slow wind, where ^{12}C:^{13}C ≈ 20 (Wannier & Sahai 1987), a ratio which itself is unusually small for a carbon star. Implications of the low ^{12}C:^{13}C ratio in the fast wind, and its evolution from the value in the slow wind, for nucleosynthesis within the central star are discussed in § 4.5.

3.1.2. HCN *and* H^{13}CN

It is difficult to determine the fractional HCN abundance in the slow wind because the emission region is compact (see § 3.2), only two HCN lines have been observed, and both are somewhat optically thick. The three most recent estimates, all of which relied solely on HCN $J = 1$–0 observations, produced radically different estimates: BGBM, assuming optically thin emission and therefore probably underestimating the ratio, estimated HCN:$H_2 = 4 \times 10^{-7}$; Sopka et al. (1989) estimated HCN:$H_2 = 3.3 \times 10^{-6}$; and NQRB estimated HCN:$H_2 > 2 \times 10^{-5}$. BGBM and Sopka et al. may also have underestimated the HCN abundance by neglecting the absorption of HCN hyperfine components of higher rest frequencies by those

of lower rest frequencies. The NQRB estimate is based upon a model which is not consistent with the HCN $J = 4$–3 intensity; as with the CO model of TB90, the NQRB model underestimates the submillimeter brightness. If the envelope were described by a single-component model, this discrepancy would imply higher temperatures and lower opacities, and therefore a lower HCN abundance than predicted by NQRB. However, the analysis is complicated by the possibility of optically thin emission from fast wind material at projected velocities near line center. A two-component model might be able to make the HCN $J = 1$–0 line very optically thick, as predicted by NQRB, and yet allow the HCN $J = 4$–3 line to be as bright as is observed because of the contribution from the warm and optically thin fast wind gas. Because the submillimeter line, and perhaps also the millimeter line, is highly optically thick, and because of the likely mixture of optically thin and optically thick emission components, it is not easy to derive an HCN abundance from the HCN line intensities.

The $H^{13}CN$ $J = 4$–3 line (see Fig. 1*e*) is somewhat more optically thick than the ^{13}CO $J = 3$–2 line; its opacity at line center is probably about unity. The HCN:$H^{13}CN$ $J = 4$–3 intensity ratio is less than the CO:^{13}CO $J = 3$–2 intensity ratio because of higher opacities in the HCN lines. The HCN $J = 4$–3 brightness temperature is less than that of the CO $J = 3$–2 brightness temperature, despite the larger HCN opacity, because the CO $J = 3$ level is excited over a larger region than the HCN $J = 4$ level. The HCN $J = 4$–3 line is much harder to excite than the CO $J = 3$–2 line, because of its much higher A-coefficient and because the HCN $J = 4$ level lies higher above the ground state than the CO $J = 3$ level.

While the HCN abundance is difficult to estimate in the slow wind, it is much easier to estimate in the optically thin fast wind. The simplest method is probably to estimate a CO:HCN abundance ratio, assuming that the two species are coextensive and similarly excited; then an HCN:H_2 ratio can be inferred from the CO:H_2 ratio. Under the assumption that both CO and HCN are in LTE at 100 K, the CO:HCN abundance ratio in the fast wind is 700. However, this is probably an underestimate. HCN, with its much larger dipole moment, is much harder to thermalize than CO, and high-J HCN levels are more likely to be subthermally populated than high-J CO levels. For this reason, we estimate a CO:HCN ratio in the fast wind of 900 ± 200. (Subthermal excitation of high-J HCN levels probably leads to a decrease in the required HCN abundance, because the opacity in the still-thermalized low-J HCN lines is then increased. If the subthermal excitation were substantial enough to affect the $J = 4$ level then the opposite effect could occur, but there is no evidence that the $J = 4$ level is subthermally populated.) Assuming CO:$H_2 = 6 \times 10^{-4}$ (TB90), then HCN:$H_2 = 7 \times 10^{-7}$ in the fast wind. This HCN:H_2 ratio is smaller than that which seems to hold in the bulk of the envelope (e.g., NQRB and discussion above).

Thus HCN seems to be less abundant in the fast wind than in the slow wind. Another way of arriving at this conclusion is to notice that the $H^{13}CN$ $J = 4$–3 and ^{13}CO $J = 3$–2 lines are about equally bright in the fast wind, as are the HCN $J = 4$–3 and CO $J = 3$–2 lines. If these species are coextensive and thermalized at the same temperature, then their opacities must be the same. But in the bulk of the envelope $H^{13}CN$ $J = 4$–3 is clearly more optically thick than ^{13}CO $J = 3$–2, and HCN $J = 4$–3 also is likely to be more optically thick than CO $J = 3$–2. Barring peculiar excitation effects, this pattern suggests that the HCN:CO ratio is higher in the slow wind than in the fast wind. We discuss possible causes of this apparent evolution in the HCN:CO abundance ratio in § 4.5.

3.1.3. HC_3N

Figure 2*a* and *b* show the $J = 38$–37 and $J = 39$–38 lines of HC_3N. The $J = 38$ level lies 307 K above the ground state. Nevertheless, this difficult-to-excite line has been detected in several circumstellar envelopes, including the PPN CRL 618 (Gammie et al. 1989) and IRC +10216 (W. E. C. J. van der Veen, private communication). Toward CRL 2688 a number of HC_3N lines have been observed, including the $J = 8$–7, 12–11, and 17–16 lines with the IRAM 30 m (BGBM), the $J = 12$–11 line with the NRAO 11 m (Jewell & Snyder 1984), and the $J = 10$–9 line by NQRB with the Berkeley-Illinois-Maryland Array (BIMA). However, the intensity of the BIMA line is lower than would be expected given the intensities of the IRAM and NRAO data, which agree with each other assuming the emission is unresolved. This discrepancy may be due to missing extended flux in the interferometer map, or perhaps to possible calibration errors. Because the IRAM observations contain more lines and have spatial resolution comparable to

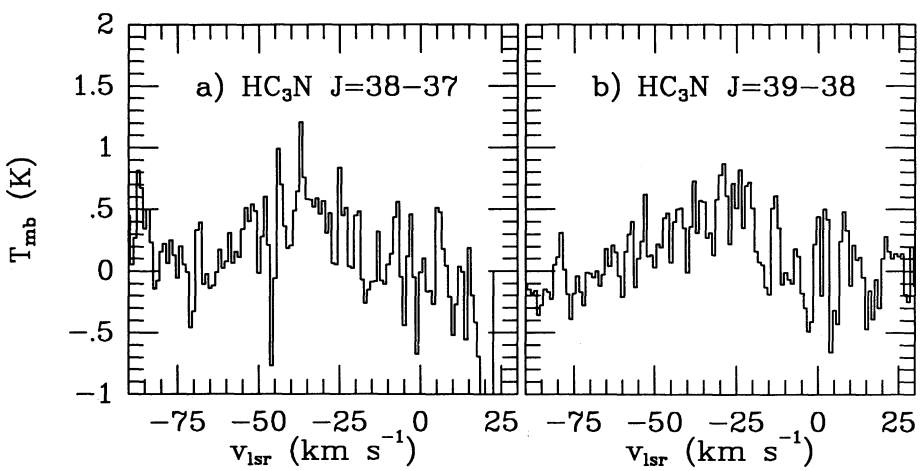

FIG. 2.—Spectra toward the central position of CRL 2688 of the (*a*) HC_3N $J = 38$–37 line and (*b*) HC_3N $J = 39$–38 line. We detected the $J = 38$–37 line with a considerably higher signal-to-noise ratio in spectra at a different LO setting. We show the spectrum in (*a*), even though the line is at the very edge of our passband, because it is our only spectrum not contaminated by emission from the CS $J = 7$–6 line.

ours, we have compared our $J = 38$–37 data with the IRAM data in order to estimate an HC_3N excitation temperature. We assume optically thin, unresolved emission. Not surprisingly, we find that no single-temperature component can fit the emission. The relative intensities of the $J = 38$–37 and $J = 17$–16 lines suggest a 90 K excitation temperature, while the lower J lines clearly sample a more abundant component with a much lower excitation temperature. An excitation temperature equal to or somewhat greater than 90 K is consistent with vibrational excitation by radiation from the infrared core, which has a temperature of 100–230 K (Ney et al. 1975; Sopka et al. 1985; Jaye et al. 1989). Alternatively, the HC_3N lines could be collisionally excited. They have a critical density of a few times 10^7 cm^{-3}, and these densities are obtained in CRL 2688 at radii where the temperature is about 100 K. The high-J HC_3N lines are broad and may be dominated by emission from the fast wind.

3.1.4. CN

Figure 3 shows spectra of the CN $N = 3$–2 hyperfine multiplet toward CRL 2688. Since each of the two principal components is dominated by hyperfine components very close together in frequency, the hyperfine splitting does not strongly perturb the shape of the line profiles. The ratio of peak intensities in the two components is about 3 : 2, approximately what would be expected for optically thin emission. The intensity ratio is lower at velocities 10–15 km s^{-1} from line center, suggesting moderate opacities. The opacities are large enough to affect the shapes of the line profiles. The $N = 3$, $J = 7/2$–$N = 2$, $J = 5/2$ line is centrally peaked and has a self-absorption feature at $-53 < v_{lsr} < -49$ km s^{-1}, which indicate moderate optical depths. The $N = 3$, $J = 5/2$–$N = 2$, $J = 3/2$ line is flat-topped, which is probably a result both of slightly lower opacities and of smearing of the line by the two principal hyperfine components.

An interesting feature of the CN line profiles is the appearance, especially in the $N = 3$, $J = 7/2$–$N = 2$, $J = 5/2$ line which is more optically thick and relatively free of smearing by hyperfine components, of weak line wings against which the blueshifted self-absorption feature appears. If high-velocity line wings exist, then CN must be abundant in the fast wind. It is not clear whether this possibility is consistent with the usual CSE chemistry models, which suggest that CN should be abundant only at larger radii where HCN can be dissociated by interstellar radiation (Glassgold et al. 1987). As the fast wind does seem to extend to relatively large radii (see § 3.2), it is probably not necessary to invoke dissociation by shocks or other processes at small radii, or to rely on the suggestion of Jura & Kroto (1990) that dissociating interstellar UV may penetrate to small radii along the low-density polar axis.

As interesting feature of the CN line wings is that, unlike the HCN and CO line wings, the redshifted wing is as bright as the blueshifted wing. However, one cannot infer a true variation in HCN : CN abundance ratio between the redshifted and blueshifted gas because, as the maps presented in § 3.2 will show, pointing offsets could create such variations in the relative intensities of the line wings.

3.1.5. CS

The CS $J = 7$–6 line (Fig. 4) is spatially unresolved and of uncertain optical depth. This line is considerably weaker than HCN $J = 4$–3, which has a similar spontaneous emission rate, probably because of both excitation effects and an abundance difference. The CS $J = 7$ level lies 65.8 K above the ground state, compared to 42.5 K for the HCN $J = 4$ level, and is thus considerably harder to excite.

The excitation of CS, and its opacity, can best be understood by comparing different lines. The only available published CS observations of CRL 2688 are in the $J = 3$–2 line, observed at IRAM by BGBM. They observed a brightness temperature only slightly less than we observe in the $J = 7$–6 lines, a difference which may be due to their larger beam. This pattern could be consistent with either optically thick or optically thin emission. Observations in a third line will be necessary to distinguish between the two cases. The absence of a clear blueshifted self-absorption feature—the spectrum in Figure 4 has a dip at the appropriate velocity, $v_{lsr} = -54$ km s^{-1}, but it is of the same magnitude as the noise—is not by itself proof that the line is optically thin.

The CS $J = 7$–6 line has prominent high-velocity line wings; this line is undoubtedly more readily excited in the warm fast wind than in the cold slow wind. Emission from the fast wind may strongly perturb the shape of the line profile even near line center.

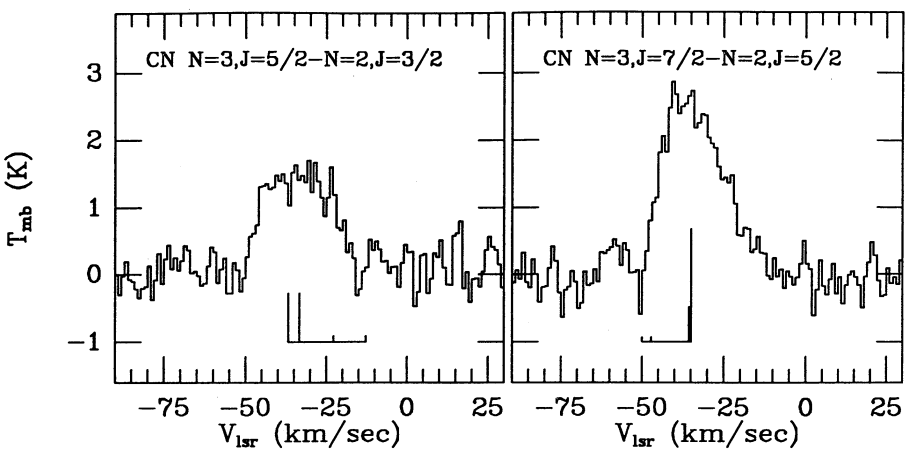

FIG. 3.—Spectrum toward the central position of CRL 2688 of the CN $N = 3$–2 lines. The left panel shows the $N = 3$, $J = 5/2$–$N = 2$, $J = 3/2$ component, the right the $N = 3$, $J = 7/2$–$N = 2$, $J = 5/2$ component. The frequencies and relative intensities of the various hyperfine components are shown in the standard way. In order to translate the abscissa to LSR velocity, we used line frequencies of 340.0334 GHz for the $J = 5/2$–3/2 component and 340.2480 GHz for the $J = 7/2$–5/2 component.

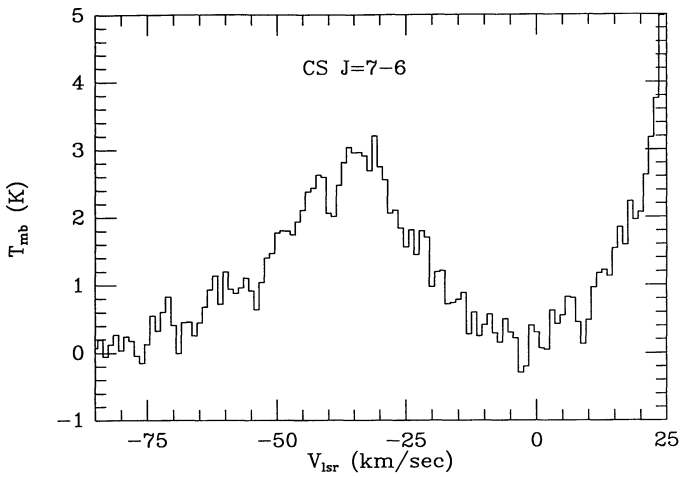

FIG. 4.—Spectrum toward the central position of CRL 2688 of the CS $J = 7$–6 line. On the redshifted side of the spectrum the redshifted edge of the CO $J = 3$–2 line (in the opposite sideband) is visible. In all of our CS spectra one of the CS line wings is blended with another line, either the blueshifted wing with the HC_3N $J = 38$–37 line or, as here, the redshifted wing with the CO $J = 3$–2 line.

3.1.6. $HN^{13}C$

Figure 5*a* and *b* shows spectra of $HN^{13}C$ $J = 4$–3; this line appeared in the opposite sideband of our $H^{13}CN$ $J = 4$–3 spectra. The $H^{13}CN$:$HN^{13}C$ intensity ratio in the $J = 4$–3 line is 31. As the $H^{13}CN$ $J = 4$–3 line is modestly optically thick, the actual abundance ratio is somewhat larger. This ratio is somewhat difficult to interpret because, according to theoretical chemistry models (Glassgold et al. 1987), the abundance ratio $H^{13}CN$:$HN^{13}C$ is not uniform throughout the envelope. However, the general trend in intensities follows the predictions of Glassgold et al.: HCN appears most abundant, CN less abundant, and HNC least abundant. A more detailed comparison with theory will probably require more extensive observational data, including ^{13}CN and HNC, and better spatial resolution.

Our detection of $HN^{13}C$ seems inconsistent with the HCN:HNC ratio of 400 estimated by NQRB. $H^{13}CN$ $J = 4$–3 is unlikely to be so optically thick as to raise the $H^{13}CN$:$HN^{13}C$ ratio this much. We note that the integrated intensity in the HNC 1–0 line observed by NQRB with an $8'' \times 7''$ beam was about 4% of the HCN 1–0 integrated intensity observed by BNQR with a $5''$ beam. The large HCN:HNC ratio estimated by NQRB arises because of the very large opacities they assumed to be present in the HCN 1–0 line. It is this same assumption which led to their comparatively large estimate for the HCN:H_2 ratio, which we discussed in § 3.1.2. It seems likely that HCN is somewhat less abundant than estimated by NQRB, that HCN $J = 1$–0 is only mildly optically thick (near line center), and that the HCN:HNC and $H^{13}CN$:$HN^{13}C$ ratios are on the order of 100. Alternatively, HNC could be relatively more abundant in the fast wind than in the slow wind. This would lead to lower HCN:HNC ratios in the $J = 4$–3 line (which is relatively more sensitive to the warm optically thin component) than in the $J = 1$–0 line (which is sensitive to the cold optically thick component).

3.1.7. HCO^+

Our failure to detect HCO^+ $J = 4$–3 is consistent with the failure by BGBM to detect HCO^+ $J = 1$–0. The central star appears insufficiently evolved to have generated HCO^+ through UV photochemistry, and such shock chemistry as may occur in CRL 2688 seems not to have generated a detectable abundance of HCO^+.

3.2. *Maps of CRL 2688*

3.2.1. *Emission near Line Center: The Slow Wind*

The submillimeter emission from CRL 2688 is quite compact, as is demonstrated by Figure 6, which shows channel maps of the CO $J = 3$–2 line. At no velocity interval is the emission much more extended than our beam. This line is the most extended of the lines we observed; other lines appear even more compact and structureless. The channel maps show no obvious evidence that emission is more extended along either the axis of the optical reflection nebulae or the optical dark lane.

However, a slight bipolarity can be found in the maps of Figure 6. Blueshifted emission is centered somewhat toward the north and east of the nebula center (see the -66 to -43 km s^{-1} velocity channels), while redshifted emission is centered toward the south and west of the nebula center (see the -30 to -1 km s^{-1} velocity channels). Difference spectra help demonstrate the reality of this bipolarity. In Figure 7 the difference

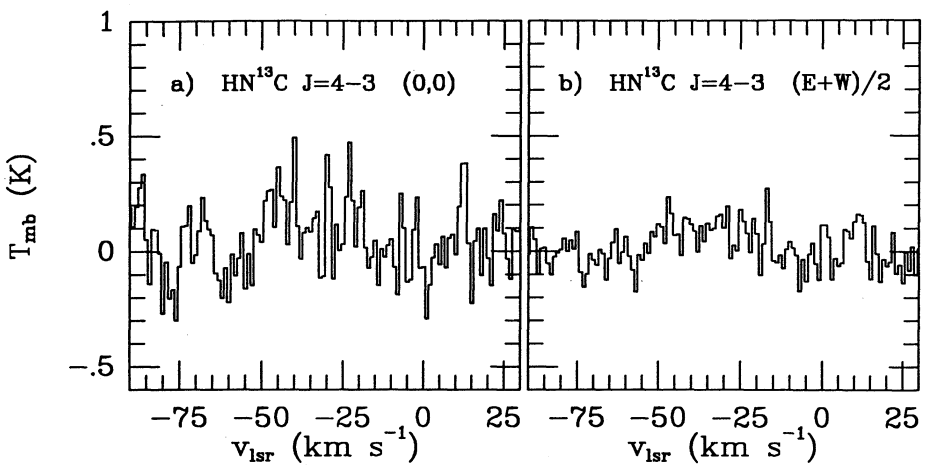

FIG. 5.—The $HN^{13}C$ $J = 4$–3 line. (*a*) Toward the central position. (*b*) Average of the spectra toward positions $6''$ east and west of the central position.

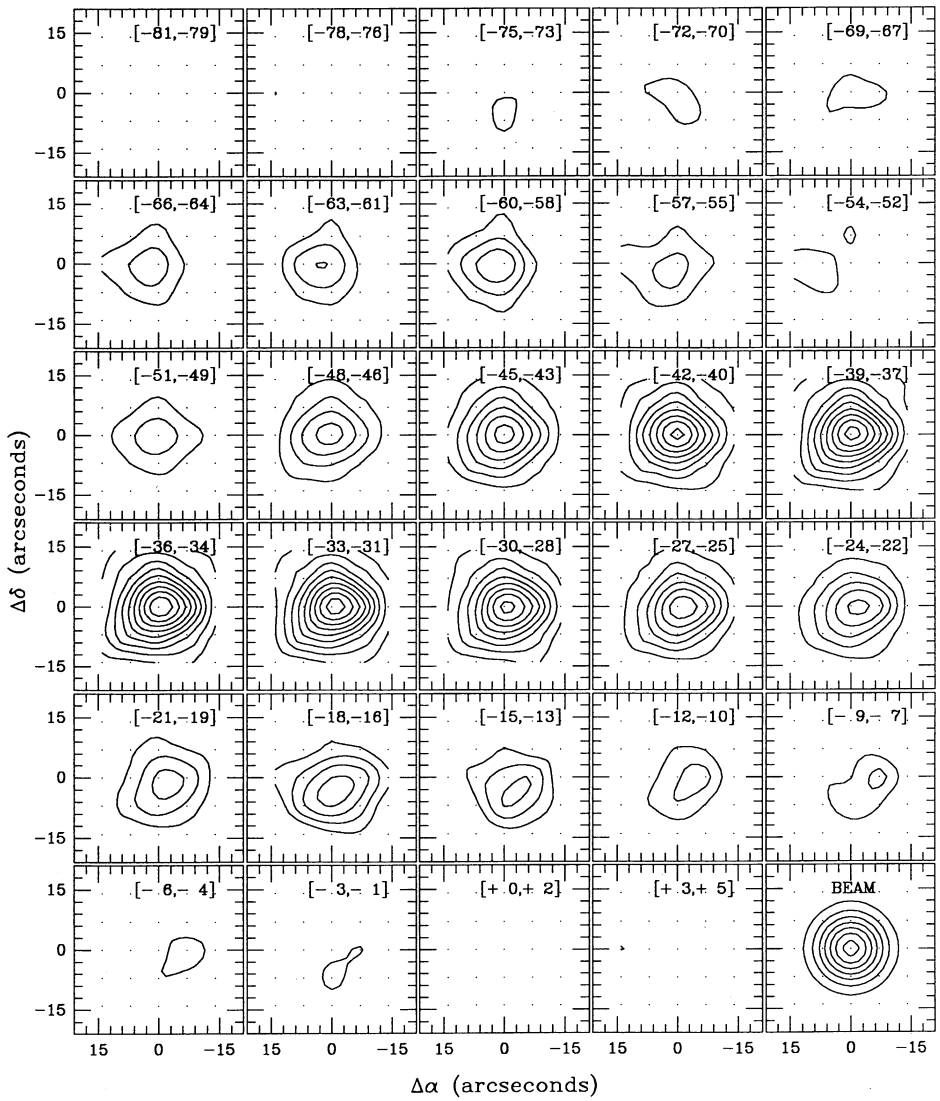

FIG. 6.—Channel maps of the CO $J = 3$–2 emission from CRL 2688. Each map presents the average emission over a 3 km s^{-1} channel. Contour levels are spaced every 1.6 K in the range -51 km s$^{-1} \leq v_{lsr} \leq -19$ km s^{-1} every 1.0 K for $v_{lsr} \leq -52$ km s^{-1}, and every 0.7 K for $v_{lsr} \geq -18$ km s^{-1}. The rms noise level in all spectra is approximately 0.3 K for 3 km s^{-1} bins.

between northern and southern spectra and between eastern and western spectra are plotted for a number of lines, with the spectra normalized by dividing by average line intensities. In all lines in which a statistically significant difference exists, the northern and eastern spectra are blueshifted from the southern and western spectra.

We detected velocity gradients in all lines except the ^{13}CO $J = 3$–2 line, the least optically thick line. It is not clear in our data that the N–S velocity gradients are larger than the E–W ones, the pattern found by BNQR. (See their Fig. 7; along the N–S axis the HCN $J = 1$–0 velocity centroid varies between -34 and -29 km s^{-1}, while along the E–W axis it varies between -32 and -30 km s^{-1}.) In all lines the shape of the difference spectra is similar, but the amplitude varies between lines. The degree to which the velocity centroid varies with position is markedly different in the different lines. The velocity centroid is strongly dependent on position in lines with a large difference spectrum amplitude, like CS $J = 7$–6, and weakly dependent on position in lines which have small difference spectrum amplitudes, like H^{13}CN $J = 4$–3 and ^{13}CO $J = 3$–2. CO $J = 3$–2 is intermediate both in difference spectrum amplitude and velocity centroid shift.

The amplitude of the difference spectrum correlates with the ratio of line wing brightness to brightness at line center. The CS $J = 7$–6 line has a ratio of peak brightness in the line wings to brightness at line center of 0.35 and has the largest amplitude difference spectra. CO $J = 3$–2 has a line wing to line center ratio of 0.26, and the next largest amplitude difference spectra. H^{13}CN $J = 4$–3 and ^{13}CO $J = 3$–2 have line wing to line center intensity ratios of about 0.18 and have the lowest amplitude difference spectra. This pattern suggests that emission from the fast wind is largely responsible for the velocity gradients.

For comparison, Figure 7*e* shows difference spectra we have formed from the observations by Smith et al. (1990) of the H_2 $S(1)$ line at 2.12 μm. These observations presumably sample interaction regions between the fast and slow winds. The shape of the vibrationally excited hydrogen difference spectra is

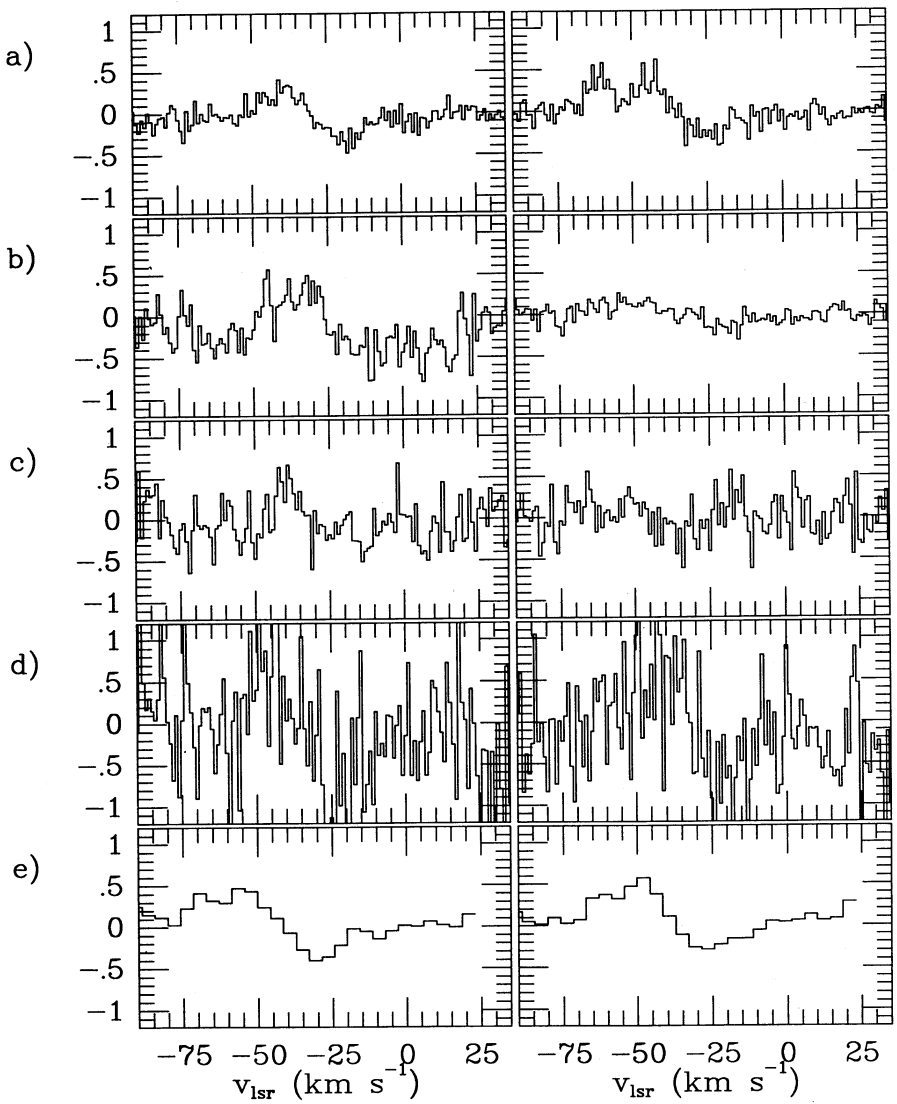

FIG. 7.—Difference spectra showing the existence of apparent velocity gradients in CRL 2688. *Left*: N/⟨N⟩ − S/⟨S⟩; *right*: E/⟨E⟩ − W/⟨W⟩. The four submillimeter lines are (*a*) CO $J = 3$–2; (*b*) $H^{13}CN$ $J = 4$–3; (*c*) ^{13}CO $J = 3$–2; (*d*) CS $J = 7$–6. In each case we show the difference between the line profile toward a position a half-beamwidth north or east of nebula center, and the line profile toward a position a half-beamwidth south or west of nebula center. Before the subtraction the line profiles were normalized by their average intensity. To convert the vertical scale to kelvin units, multiply by the average intensities: 5.39 K for CO, 2.36 K for $H^{13}CN$, 1.88 K for ^{13}CO, and 0.97 K for CS. For comparison, in (*e*) we present N–S and E–W difference spectra from the H_2 $S(1)$ line observations of Smith et al. (1990). The vertical scale in (*e*) is in units of 10^{-16} W cm^{-2} μm^{-1}.

remarkably similar to the shape of the molecular line difference spectra, especially after accounting for the 12 km s^{-1} velocity resolution of the Smith et al. data. This, too, suggests that the fast wind may be responsible for the velocity gradients observed in millimeter and submillimeter wavelength lines. As we will discuss in § 3.2.2, our maps of the fast wind show a clear pattern of blueshifted emission in the east and north and redshifted emission in the west and south.

3.2.2. *The Fast Wind*

Figure 8 presents a map of the CO $J = 3$–2 blueshifted and redshifted high-velocity line wings. The emission is integrated over -64 km $s^{-1} < v_{lsr} < -54$ km s^{-1} in the case of the blueshifted line wing (*solid contours*) and -17 km $s^{-1} < v_{lsr} < -7$ km s^{-1} in the case of the redshifted line wing (*dashed contours*). The rms deviation from zero in 10 km s^{-1} wide bins, calculated in regions of our spectra which we believe to be free of line emission, is 0.19 K, and the contours shown in Figure 8 are multiples of 0.38 K, or 2 σ. This σ includes contributions from baseline errors as well as random noise.

Structure is readily discernible in this map. First, the fast wind emission is somewhat extended. The rate of radial fall-off in intensity is substantially slower than is consistent with emission from a point source. Second, the fast wind seems to be more extended along the N–S and E–W axes than along other directions. Third, there is a strong asymmetry between the blueshifted and redshifted components of the fast wind. The blueshifted line wing emission is much stronger than the redshifted emission north and east of nebula center, while the reverse is true south and west of nebula center. For instance, at the map point which is nominally 7″ east of nebula center, the blueshifted line wing intensity is 12 σ while the redshifted line

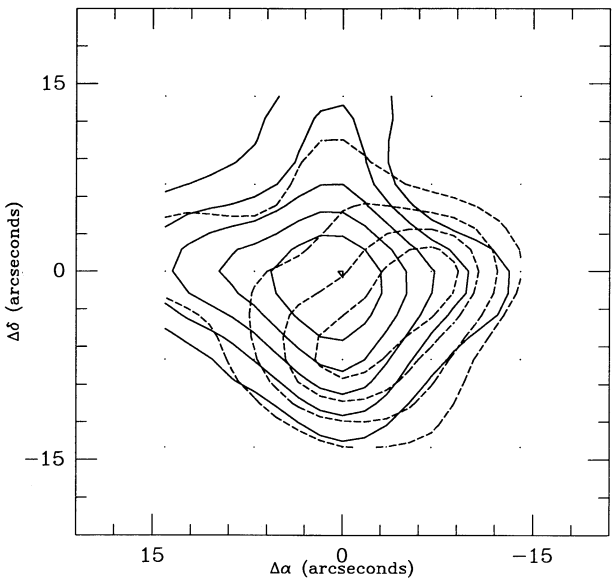

FIG. 8.—Map of CO $J = 3$–2 high-velocity line wing emission from CRL 2688. Solid contours represent average intensity between -64 km s$^{-1} < v_{lsr} < -54$ km s^{-1} (the blueshifted wing) and dashed contours average intensity between -17 km s$^{-1} < v_{lsr} < -7$ km s^{-1} (the redshifted wing). The contour levels are multiples of 0.38 K. The rms noise level is 0.19 K for 10 km s^{-1} bins.

wing intensity is only 4 σ. At the map point which is nominally 7″ west of nebula center, the blueshifted line wing intensity is only 6 σ while the redshifted line wing intensity is 9 σ. A similar asymmetry exists along the N–S axis.

Other observations, including some with higher spatial resolution, have also detected an E–W bipolarity in the fast wind. The -11.5 km s^{-1} and -48.5 km s^{-1} panels of BNQR's Figure 4 show that the blueshifted line wing emission peaks about 4″ ENE of the redshifted line wing emission. Similarly, Figures 4*b* and 4*e* of TB90 also show the redshifted line wing emission peaking to the west of the blueshifted emission. It is not easy to tell from the published figures, which cover limited velocity ranges, that our data are completely consistent with theirs. Nevertheless, there seems to be conclusive observational evidence that the CRL 2688 fast wind is extended and has large velocity gradients along the E–W axis as well as along the N–S axis.

Our map of the fast wind shown in Figure 8 suggests that the fast wind consists of two distinct bipolar winds, one extended along the N–S axis and one along the E–W axis. This was the pattern observed in H_2 $S(1)$ emission by Smith et al. (1990); they detected four lobes of emission, two along the N–S axis in which a blueshifted emission lobe lies north and a redshifted lobe south of the central star, and two along the E–W axis in which a blueshifted lobe lies east and a redshifted lobe west. We have investigated the morphology of the fast wind by convolving model brightness distributions with our beam and plotting the results using the same plotting package which produced Figure 6. The best-fit distribution of the CO $J = 3$–2 line wing emission is strikingly similar to the H_2 $S(1)$ brightness distribution observed by Smith et al. (1990).

4. DISCUSSION

As a picture of the morphology of CRL 2688 is essential in interpreting our data, let us begin the discussion by trying to imagine a morphology which is consistent with all published observations.

4.1. *The Morphology of CRL 2688*

4.1.1. *The Distribution of Densities in the Envelope*

Optical and infrared continuum observations show that the CRL 2688 has a bipolar appearance on both small and large size scales. Bipolarity in the optical reflection nebula, for instance, is visible at radii from 1″ to more than 10″ (Ney et al. 1975). On small spatial scales, 11–18 μm observations by Danchi et al. (1991) with about 1″ resolution show that the mid-infrared continuum emission, which is sensitive to dust temperature, is elliptical in shape. The major axis is aligned with the optical reflection nebulae and has length 5″, while the minor axis is aligned with the optical dark lane and has length 3″. The observations of Danchi et al. have better spatial resolution and a better instrumental point-spread function than the observations of Jaye et al. (1989). As emission contours within 1″ of the central star share this pattern, these observations indicate that aspherical mass loss is ongoing. Probably the current mass loss, like earlier mass loss, has high densities (and low temperatures) in an equatorial plane which we see edge-on and aligned with the E–W axis, and low densities (and high temperatures) along its symmetry axis, which is nearly aligned with the N–S axis. High densities are associated with low temperatures because high dust densities inhibit the outward propagation of warming radiation from the central star and high gas densities lead to effective cooling by molecular line radiation.

Observations of molecular lines at radio and millimeter wavelengths tend to be somewhat insensitive to these density variations. On physical grounds one would expect optically thin lines and optically thick but subthermally populated, collisionally excited lines to appear elongated along the high-density E–W axis, and optically thick, thermalized lines to appear most extended along the warmer N–S axis. Unfortunately most of the high-resolution molecular observations have been made in lines which are thermalized and moderately optically thick. In these lines the effect of larger gas columns along the high-density axis is somewhat compensated by two competing effects. First, the higher temperatures along the low-density axis will tend to increase emission there. Second, the lower densities affect the excitation of high-J levels much more strongly than the low-J levels and lead to a decrease in the partition function and an increase in the opacity of low-J levels, without necessarily reducing the excitation temperature of the low-J levels substantially. Partly because of these effects, and partly because of inadequate spatial resolution, the deviations from spherical symmetry in molecular line maps have, with rare exceptions, been slight. Kawabe et al. (1987) found CO $J = 1$–0 emission to be extended along the E–W direction, coincident with the optical dark lane, while Heiligman et al. (1986) found CO $J = 1$–0 emission to be extended along the N–S direction. VLA observations by Nguyen-Q-Rieu, Winnberg, & Bujarrabal (1986) found the (1, 1) inversion line of NH_3 to be elongated in the E–W direction, but with a narrow spur aligned with the N–S axis. NQRB found emission in $H^{13}CN$, HC_3N, and HNC to show weak deviations from spherical symmetry, in the form of slight elongation in the E–W direction. None of these observations contradict the interpretation derived from the optical and infrared data that the envelope is dense along an equatorial plane which we see

edge-on along the E–W axis, and more tenuous along the N–S symmetry axis.

The radial distribution of the density is not so clear. The molecular observations lack sufficient spatial resolution and coverage of the rotational ladder to determine the density as a function of radius. Infrared observations may be able to do better at small radii. The mid-infrared emission was interpreted by Jay et al. (1989) as thermal emission from a mildly extended source in which the temperature is independent of radius. The morphology which would most easily reproduce this result is a thin shell located at a radius of 1″, with an empty inner cavity. It was this model morphology which led Jura & Kroto (1990) to conclude that CRL 2688 had evolved off the AGB 200 yr ago, under the assumption that a sharp decrease in mass-loss rate would have occurred at that time. All of these interpretations are dubious. The brightness distribution observed by Jaye et al. was virtually identical to their instrumental point-spread function, and it is not clear that they could have resolved a radial dependence of the dust temperature, if one existed. The recent mid-infrared observations of Danchi et al. (1991) have sptially resolved the infrared emission and show no evidence for a thin shell of emission. Rather, they indicate that mass loss has been continuous and is ongoing. Moreover, the assumption that the mid-infrared emission is necessarily thermal is called into question by observations showing that nonthermal emission from UV and optically excited tiny grains can dominate the mid-infrared continuum near stars with $T_* > 5000$ K (Sellgren, Luan, & Werner 1990). Color temperatures from this nonthermal emission are naturally independent of radius. Evidence that nonthermal emission is present is provided by Geballe et al. (1992), whose infrared spectra of CRL 2688 show lines associated in other sources with nonthermal emission from tiny grains or large molecules.

4.1.2. *The Distribution of Expansion Velocities*

Though the density distribution seems to be simple, the velocity distribution is complex and poorly understood. There are grounds for believing that the expansion velocity may vary both with radius and polar angle. Even nonradial motions may exist; Nguyen-Q-Rieu et al. (1986) observed peculiar line profiles in ammonia inversion lines which they suggested might be due to an outflow from the dense equatorial plane superposed on the outflow from the central star, and BNQR have suggested that the envelope is rotating.

First let us consider the dependence of the expansion velocity upon radius. On theoretical grounds one might expect the expansion velocity to have increased as the central star evolved away from the AGB, mainly because the stellar radius has shrunk by more than a factor of 10 in that time. Because of this shrinkage the escape velocity from the central star, assuming a core mass of 0.7 $M_\odot$, has risen from about 15 km s^{-1} when the central star was on the AGB to about 60 km s^{-1} at present. A rule of thumb derived from observations is that wind expansion velocities tend to scale with the stellar escape velocity, with a proportionality constant that is a slow but monotonically increasing function of stellar temperature (e.g., Pauldrach et al. 1988). This rule of thumb would suggest that the wind expansion velocity will have increased by more than a factor of 4 since CRL evolved off the AGB.

A further argument for a recent increase in the expansion velocity comes from the standard ideas about the mechanisms driving mass loss from evolved stars. Mass loss is probably caused by a two-part mechanism (Lafon & Berruyer 1991). Some undetermined mechanism(s) eject stellar material to at least the radius where dust forms. This radius corresponds to a temperature on the order of 1200–1500 K and can be as little as $2.5R_*$ for an AGB star, but is more than $30R_*$ for CRL 2688. Beyond this radius radiation pressure on dust accelerates the gas, and radiation pressure ultimately determines the asymptotic expansion velocity (Knapp 1986). In this picture, it is natural to suppose that CRL 2688's mass-loss rate has declined since it evolved off the AGB, since the mechanism which ejects matter to the radius of dust formation is likely to be less effective now that the stellar radius is smaller. Moreover, since the central star evolved off the AGB its UV luminosity has increased significantly, as post–AGB evolution occurs at roughly constant luminosity but rapidly increasing stellar temperature, and UV radiation couples more effectively to dust than infrared radiation. Thus the radiation pressure on dust has increased at the same time that the inertia of the wind has probably decreased. This combination is likely to result in an increased wind expansion velocity.

Observations are consistent with radial dependence in the expansion velocity, subject to one caveat. The parabolic shape of most molecular line profiles indicates that the bulk of the gas in the dense equatorial plane is expanding at a velocity on the order to 16–19 km s^{-1}. Thus, any upward evolution in the wind expansion velocity must have begun relatively recently, probably within the last 400 yr. If CRL 2688 evolved off the AGB 200 yr ago, as Jura & Kroto (1990) suggest, and the wind expansion velocity along our line of sight to the center of the nebula has increased over that time from 18 to 50 km s^{-1}, then material which could contribute to the molecular line wings would have reached a radius of at most 3×10^{16} cm $\approx 2''$. The available observations are consistent with the possibility that *all* gas within this radius is rapidly expanding. The molecular maps (discussed in § 3.2) indicate that both slowly and rapidly expanding gas exist at radii of 2″–6″.

Variations in the width of the blueshifted self-absorption feature between different lines may indicate evolution in the slow wind expansion velocity at larger radii. The CO $J = 1$–0 and $J = 2$–1 features are 1–2 km s^{-1} wide and centered near $v_{\rm lsr} = -55$ km s^{-1} (Kawabe et al. 1987; Young et al. 1991; TB90). The CO $J = 3$–2 feature is about 4 km s^{-1} wide and is centered near $v_{\rm lsr} = -54$ km s^{-1}. The HCN $J = 4$–3 feature is about 5 km s^{-1} wide and is centered near $v_{\rm lsr} = -52.5$ km s^{-1}. The common pattern is that the higher the excitation of the line—and, therefore, the smaller the radius at which absorption begins—the broader the absorption dip becomes and the closer to line center its inner edge moves. This evolution suggests that the expansion velocity may have decreased from about 20 km s^{-1} at large radii to perhaps 16 km s^{-1} at the radius where the HCN $J = 1$ level becomes subthermally populated. (Young et al. 1992 have proposed an alternative explanation for the shapes of the self-absorption features, which relies on absorption of slow wind material against fast wind emission which is spatially extended in the plane of the sky but not along our line of sight. As our observations show that the fast wind is indeed spatially extended in this way, the Young et al. model is certainly plausible.) A pattern of decreasing expansion velocity, with decreasing radius at relatively large radii, would be consistent with the idea that the time span of bipolar mass loss at rates greater than 10^{-4} $M_\odot$ yr^{-1} is short, perhaps 1000 yr, and that the expansion velocity decreases as the mass-loss rate increases from the 10^{-5} $M_\odot$ yr^{-1} rates typical of late AGB stars. In NGC 7027, there is

evidence for a similar pattern: that gas at large radii is characterized by smaller mass-loss rate, and perhaps, also larger expansion velocities, than the gas at smaller radii (Jaminet et al. 1991).

The notion that the expansion velocity varies with polar angle has mainly theoretical support. The theoretical argument is that, if radiation pressure determines the ultimate expansion velocity, then the low mass-loss rate directions will tend to acquire larger expansion velocities. The direct observational evidence is limited. Morris et al. (1987), in observations of the bipolar nebula OH 231.8+4.2, found that its fast wind is extended and bipolar, while its slow wind is compact and unresolved. Morris et al. suppose the slow wind to consist of a disk and the fast wind to be collimated orthogonal to the disk. However, this interpretation is unproven.

A number of authors have adopted the view that the fast wind in CRL 2688 is strongly collimated along the low-density N–S axis. Evidence in support of this view may be provided by the NH_3 observations of Nguyen-Q-Rieu et al. (1986), who found that ammonia emission is largely concentrated in the E–W equatorial plane, but found also a narrow northern spur which was aligned with the low-density axis and was unresolved by the VLA. Authors who have supposed the fast wind to be highly collimated have often gone on to estimate the expansion velocity of the fast wind by dividing the observed half-width of the line wings by the sine of the inclination angle of the low-density axis. Thus, for instance, Young et al. (1992) suggest that the deprojected outflow velocity of the CRL 2688 fast wind may be as much as 360 km s^{-1}. In our view this analysis is not indicated by the observational data. If the envelope were characterized by a highly collimated fast wind expanding at some characteristic velocity, the line profiles would resemble the profile which Trams et al. (1990) found toward the peculiar star HD 101584. That is, there would be sharp peaks in emission at velocities redshifted and blueshifted from line center by the product of the wind expansion velocity and the sine of the inclination angle. This is not the sort of line profile which CRL 2688 and most other bipolar nebulae show. On the contrary, in CRL 2688 the line wings show a continuous distribution of emission, with the intensity increasing as the velocity nears line center. This distribution of intensities could conceivably be caused by a collimated fast wind if the amount of material expanding at a given velocity is continuous and monotonically decreasing function of expansion velocity. However, the most likely explanation for the observed shape of the line profiles is that the fast wind is flowing in all directions. The fast wind may well be more extended along low-density directions than high-density directions, and the expansion velocity may well be larger along low-density directions, but the divergence in radial extent and expansion velocity need not be large to account for the observed spectral line profiles.

In summary, there have been two leading models for the morphology of the CRL 2688 fast wind. In one, the radial variation in expansion velocity is regarded as dominant, and the fast wind therefore is approximately spherically symmetric and lies at small radii. In the other, the variation in expansion velocity with polar angle is regarded as dominant, and the fast wind therefore is bipolar and is extended only along the polar axis. Young et al. (1992), for example, considered both these models. We now propose a third model for the fast wind: that it consists predominantly of four blobs of rapidly expanding material ejected in bipolar fashion during two discrete mass loss episodes.

4.1.3. *High-Velocity Blobs*

Our observations have produced three new pieces of evidence about the origin and nature of the fast wind material. First, the temperature of the fast wind material is quite high, on the order of 100 K. This indicates either that fast wind material lies within a few arcseconds of the central star, or that the fast wind is strongly heated by shocks or collisions as it streams into or through more slowly expanding material. Second, our map of the high-velocity line wings suggests that the fast wind material does not lie only at small radii, but also at rather large radii. It seems likely that much of the emission comes from near the four lobes of H_2 $S(1)$ emission seen by Smith et al. (1990). Third, the evolution of the ^{12}C:^{13}C ratio between the slow wind and fast wind is strong evidence that most if not all of the fast wind material was lost at a later epoch than most of the slow wind material. The fast wind material seems to have undergone much more extensive CN processing than the slow wind material. As CN processing occurs in a thin layer just outside the core, heavily CN processed material would probably be lost only when the core has nearly been exposed by mass loss. This near exposure of the core occurs in the PPN stage, not the AGB stage. If material in or near the H_2 $S(1)$ lobes represents the dominant source of the line wing emission, and was lost during the PPN stage as the ^{12}C:^{13}C ratio indicates, the lobe material must have been ejected with expansion velocities greater than 100 km s^{-1} in order to have obtained its present radii.

Ejection of high-velocity blobs or bullets seems to have occurred in other bipolar nebulae and PNs. The very young PN M2–9 has several knots ejected in bipolar fashion that show very large proper motions (Kohoutek & Surdej 1980). The PNs NGC 2440 and NGC 6210 show bipolar knots (e.g., Icke, Preston, & Balick 1989). Many PNs show bipolar ansae which may have been produced by highly collimated bipolar mass loss episodes. Among PPNs the F-type post–AGB star HD 101584 has bright spectral bumps shifted 40 km s^{-1} and 130 km s^{-1} from line center on both the redshifted and blueshifted sides of its CO $J = 1$–0 line profile (Trams et al. 1990). These spectral bumps likely represent emission from blobs or collimated jets ejected in bipolar fashion and having considerable mass. As no isolated spectral bumps of the type seen by Trams et al. are apparent in the spectra of CRL 2688, these postulated blobs must reside within about 20° of the plane of the sky (if they are expanding at 50 km s^{-1}) or have developed a very large velocity dispersion. Smith et al. (1990) found that the emission from these blobs peaked 10–15 km s^{-1} from the nebular rest velocity, but that the emission has a broad profile extending to about 50 km s^{-1} from the nebular rest velocity.

Passage of high-velocity blobs through the envelope would disturb and heat the nearby slow wind material. The disturbance caused by the ejection of the blobs would be most apparent at large radii, near the blobs themselves. The pressure gradient between low-density regions swept clear of gas by the passage of the blobs and the surrounding dense slow wind would accelerate the slow wind material to transverse velocities $v \approx (2P/\rho)^{1/2} \approx (T/100\ \mathrm{K})^{1/2}$ km s^{-1} where P is the pressure, ρ the density, and T the temperature in the slow wind material. At small radii, where the width of the blobs would be comparable to the diameter of the central star, about 10^{13} cm, an evacuated wake would be filled in by slow wind material in about 3 yr and the disturbance caused by the passage of a blob would probably have decayed by now. At large radii, where the

size of the H_2 $S(1)$ emission regions indicates that the width of the blobs may have grown to as much as 10^{16} cm, the lifetime of a disturbed, low-density wake might be on the order of centuries. Turbulence in such a region could lead to heating of the gas.

4.2. *Velocity Gradients: Due to Rotation or Envelope Asymmetries?*

In order to account for the observed velocity gradients along the E–W axis, BNQR proposed that the envelope is rotating. At the time of their work there was no strong evidence for deviations from axial symmetry in CRL 2688, and, if CRL 2688 is axially symmetric, the only possible cause for E–W velocity gradients is rotation. However, the evidence is no longer consistent with the assumption of axial symmetry. Both the Smith et al. (1990) observations and our map of the line wing emission indicate the existence of hot, rapidly expanding material that appears blueshifted on the east side of the envelope and redshifted on the west, and which definitely (in the case of the H_2 line) or probably (in the case of the submillimeter lines) emits at projected velocities close to line center.

There are many possible reasons why the velocity centroid of a line might vary with position in observations toward a circumstellar envelope. One is rotation of the envelope. Envelope asymmetries can also cause such an effect. For instance, in NGC 7027 the velocity centroid of CO line profiles shifts dramatically with position due to an asymmetry in mass loss (Jaminet et al. 1991). In NGC 7027, the CO $J = 3$–2 line, observed in a 14″ beam toward a point 10″ NW of the nebula center, has a velocity centroid of $+28.0$ km s^{-1}, while the same line observed 10″ SE of nebula center has a velocity centroid of $+24.8$ km s^{-1}. The lines NE, SW, and toward nebula center have velocity centroids of about $+26.5$ km s^{-1}. Comparison of the CO $J = 3$–2 line with the $J = 1$–0 line shows that the $J = 3$ level is subthermally populated on the blueshifted side of the envelope NW of nebula center and on the redshifted side of the envelope SE of nebula center. Despite the variation of the velocity centroid along the NW–SE axis, there is no real velocity gradient in NGC 7027; so far as we know all the gas is expanding radially with a uniform expansion velocity.

We mention the example of NGC 7027 only to emphasize that envelope asymmetries must be considered, and ruled out, before rotation can be inferred from velocity gradients. We now turn to a discussion of possible causes for the velocity gradients in CRL 2688. We begin by considering the gradient along the axis of the optical reflection nebula.

4.2.1. *The North–South Gradient*

In CRL 2688 the velocity gradient along the symmetry axis of the optical reflection nebula is generally agreed to be due to the envelope asymmetry. However, the conventional explanations for the N–S gradient are not without problems. According to the model of Yusef-Zadeh et al. (1984), the northern lobe of the reflection nebula lies mostly on the blueshifted side of the envelope, and the southern lobe lies mostly on the redshifted side. These lobes are regions of unusually low density. The millimeter and submillimeter-wavelength observations show that on the north blueshifted emission is brighter than redshifted emission, while on the south redshifted emission is brighter. Thus it seems the low-density gas is brighter than the high-density gas.

It is not easy to explain this pattern. Remember that the opposite pattern holds in NGC 7027, where high-density regions are brighter than low-density ones (Jaminet et al. 1991) due to their higher collisional excitation and larger molecular columns. It is conceivable that certain other effects might lead to velocity gradients of the appropriate sign. For instance, high-density regions tend to be colder than low-density regions. Also, the partition function is reduced in low-density regions, increasing the fraction of gas which lies in low-J levels, and this increase in opacity partially compensates for the larger molecular columns in high-density regions. Furthermore, the low-density directions might have higher expansion velocities than high-density directions. BNQR suggested that the variation of expansion velocity with mass-loss rate might cause the N–S velocity gradients. However, this is not so clear, because the effects of a change in expansion velocity are quite complex. A larger expansion velocity leads to changes in excitation, because the density is inversely proportional to the expansion velocity and kinetic temperature also depends on the expansion velocity. Also, the lowest order effect of an increased expansion velocity on (for example) the blueshifted side of the envelope is not to increase the blueshifted emission, but rather to stretch out the blueshifted emission toward higher velocity shifts. This can lead to a blueward shift in the line velocity centroid, but would not make the blueshifted side of the envelope intrinsically *brighter* than the redshifted side, which is what is observed.

An explanation for the velocity gradient along the N–S axis that is free of these difficulties is that the N–S gradient is caused by the N–S asymmetry in the fast wind. Fast wind material which lies near the plane of the sky and therefore emits near line center could itself create the gradients. Alternatively, the passage of the putative high-velocity blobs through the slow wind material may have heated the gas to produce a temperature asymmetry which might account for the observed velocity gradient. The idea that the excess emission which leads to the observed velocity gradients arises from an interaction region between fast and slow wind material is consistent with the data presented in § 3.2, especially the observation that the difference spectra in Figures 7*a*–7*d* have similar velocity profiles to difference spectra of the vibrationally excited molecular hydrogen line emission observed by Smith et al. (1990) and shown in Figure 7*e*.

4.2.2. *The East–West Gradient*

The proposal by BNQR that the envelope is rotating about the symmetry axis cannot explain the observed E–W asymmetry in the fast wind, because the required orbital velocity of the fast wind material would be unphysically large. The rotation hypothesis is viable as an explanation of the pattern of emission at velocities near line center. But it is an ad hoc explanation which accounts for neither the E–W asymmetry at more extreme velocities, nor for the N–S velocity gradient which is so similar to the E–W gradient. A more natural explanation is that the E–W velocity gradient is caused by emission from the high-velocity blobs postulated in § 4.1.3, or by emission from surrounding gas disturbed, heated, and perhaps accelerated by the passage of the blobs. This explanation is the same as that we suggest for the N–S velocity gradients and accounts for the observed gradients at all velocities.

4.3. *Temperature Distribution of the Envelope*

The compactness of emission from the slow wind is probably not due to subthermal excitation of CO at small angular radii; rather, it is likely that the kinetic temperature itself is very small except at the smallest radii. The low densities required if the excitation is to be subthermal are inconsistent with the

large observed molecular abundances, unless fractional abundance ratios such as the CO:H_2 ratio are anomalously high. However, the coldness of the envelope is consistent with predictions of thermal balance models (Kwan & Linke 1982; Sahai 1990), in which CSEs formed by very large mass-loss rates are cold, because the high densities make for effective cooling by molecular line radiation and ineffective heating due to gas-dust collisions. For CRL 2688, TB90 have calculated a kinetic temperature distribution from a thermal balance model, with free parameters adjusted to agree with IRAM observations of CRL 2688 in the CO 1–0 and 2–1 lines. Their kinetic temperature distribution falls rapidly with radius near the central star, like $r^{-1.5}$, and reaches a kinetic temperature of 15 K at a radius of 8×10^{16} cm (corresponding to only 5″ at 1 kpc). This kinetic temperature is sufficiently small to make CO $J = 3$–2 line emission weak.

It is clear that the picture of the CRL 2688 envelope derived by TB90 is qualitatively correct. The envelope becomes cold at an angular radius of a few arcseconds, accounting for the limited spatial extent of the submillimeter line emission. The rate of radial decrease in the kinetic temperature slows abruptly as a temperature of about 10 K, accounting for the more extended emission seen in CO $J = 1$–0.

We have compared our observed CO line profiles with line profiles calculated using a model identical to that of TB90. Our model differs slightly from the published description of the TB90 model: a typographical error in the TB90 paper caused the diameter of the central infrared core to be described as the radius. The actual TB90 calculations used the correct infrared core size (Truong-Bach, private communication). Our comparison indicates that the TB90 kinetic temperature distribution is too cold to account for the observed CO $J = 3$–2 line intensity. Calibration differences between the IRAM and JCMT data could account for some of this discrepancy, but the observations of Young et al. (1992) support the JCMT calibration. A more likely explanation for the discrepancy is that the TB90 model has neglected some important features of the envelope. In their model the envelope consists of a single, spherically symmetric component: the dense, cool slow wind.

A similar discrepancy between the line intensity predictions of models based on low-J CO observations and the high-J CO observations existed for the AGB star IRC +10216. This discrepancy has generally been attributed to a decrease in the IRC +10216 mass-loss rate from 5–10×10^{-5} $M_\odot$ yr^{-1} a few thousand years ago to about 2–3×10^{-5} $M_\odot$ yr^{-1} currently (see, for instance, Sahai 1987, and references therein). This decrease in mass-loss rate greatly increases the ratio of high-J to low-J intensities at small radii, because the lower mass-loss rates make for higher temperatures. In the limit of low opacity and high temperature—appropriate for IRC +10216 in the $J = 1$–0 line at small radii—CO $J = 1$–0 brightness temperature varies as T^{-1}, while the high-J CO line brightness temperatures tend to increase as T increases. Thus, the hot, low mass-loss rate inner envelope model is effective at increasing the high-J to low-J line intensity ratios. Something similar could contribute to the discrepancy between the CO $J = 3$–2 observations in CRL 2688 and the predictions of the TB90 model. Indeed, it is natural to suppose that the mass-loss rate in CRL 2688 may have decreased in recent centuries as the central star evolved off the AGB.

However, our model calculations indicate that, even if radial variations in mass-loss rate are allowed, spherically symmetric models cannot readily account for the shapes of the CO line profiles. (TB90 fit only the emission at line center, perhaps because of this problem.) It is especially difficult to make the CO $J = 1$–0 line profile as strongly centrally peaked as is observed. To make the $J = 1$–0 profile match its observed shape, a spherically symmetric envelope with uniform mass-loss rate would have to be extremely optically thick, requiring a mass-loss rate and/or CO:H_2 ratio considerably higher than even the values estimated by TB90. Such high opacities would force the line intensities to decrease with increasing J, contrary to the observed progression of line intensities. Moreover, any increase in the model mass-loss rate would lead to more effective cooling of the envelope, decreasing the model temperature and further exacerbating the discrepancy between model and observed intensities. This last problem is especially piquant in that the TB90 model significantly underestimates the rate of cooling by molecular line radiation. TB90 included only cooling due to CO transitions in their model, but at small radii, where most of the cooling occurs, the cooling rate from other molecules is greater than that from CO. Our observations show that the CO $J = 3$–2 line at 345 GHz contributes less than 25% of the cooling by molecular line radiation in the 330–360 GHz window. Cooling from CO may represent about 10% of the total cooling by molecular line radiation at small radii.

How can these difficulties be resolved? A successful model must include both important emission components: the dense, cold, optically thick slow wind and the warm, optically thin fast wind. In the submillimeter both of these components contribute significantly to the emission seen within 20 km s^{-1} of line center. CO $J = 3$–2 emission is brighter than CO $J = 2$–1 emission due to the contribution from the fast wind, which is a rapidly increasing function of J. The line profiles are centrally peaked partly because of the deviation from spherical symmetry in the envelope, in which the lowest density (and therefore warmest) regions, and also regions heated by the putative blobs, lie more or less in the plane of the sky, while dense (and therefore cold) gas lies along our line of sight. Another important effect tending to make the line profiles more centrally peaked is the possibility of absorption by slow wind material against fast wind material in the plane of the sky; the work of Young et al. (1992) emphasizes the importance of this effect. A final possibility is that the slow wind may in fact be *colder* than the TB90 model predicts, a possibility which is consistent with the omission of non–CO cooling lines from the TB90 model and TB90's neglect of contaminating emission from the warm, optically thin fast wind. Then, if the slow wind emission is relatively more dominant at velocities 15 km s^{-1} from line center than at line center, the line profile would tend to be more centrally peaked than predicted by the TB90 model.

4.4. *Mass-Loss Rates*

Given the absence of a clear understanding of the temperature and morphology of the CRL 2688 envelope, only crude estimates of the mass-loss rate for the slow wind have been possible. These estimates ultimately come down to (1) assuming a CO:H_2 ratio based on observations of other circumstellar envelopes or of C:H and O:H ratios in PNs, and then (2) finding a mass-loss rate which would produce sufficient CO to reproduce the observed opacities in the CO lines. CRL 2688 seems to be optically thick in the CO lines, and therefore very high mass-loss rates, around 1.5×10^{-4} $M_\odot$ yr^{-1} or larger, are necessary if a standard CO:H_2 ratio is assumed (Knapp & Morris 1985; TB90).

We are in a much better position to estimate the mass of the fast wind material, because the fast wind emission is optically

thin. The integrated intensity from an optically thin line in LTE at a temperature T is

$$W = \int T_R \, dv = \frac{8\pi^2 \nu S \mu^2}{3k} \frac{N e^{-E_u/kT}}{Z},$$

where T_R is the Rayleigh-Jeans brightness temperature of the source, ν is the line frequency, S is the line strength, μ is the dipole moment, N is the beam-averaged column density, E_u is the energy relative to the ground state of the upper level of the transition, and Z is the partition function (e.g., Cummins, Linke, & Thaddeus 1986). For CO that is thermalized at high temperatures, $Z \approx 2kT/h\nu_{1-0}$, where ν_{1-0} is the frequency of the $J = 1$–0 transition. The total number of CO molecules subtended by the beam is the product of the column density and the area subtended by the beam, which is $A = \pi D^2 B^2/(4 \ln 2)$ for a telescope beam with FWHP angular diameter B and source distance D. If the fast wind is unresolved, its total mass is

$$M_{fw} = \frac{\pi}{4 \ln 2} \frac{D^2 B^2 m_{H_2}}{f_{CO:H_2}} \frac{3kW}{8\pi^3 \nu S \mu^2} e^{E_u/kT} \frac{2kT}{h\nu_{1-0}},$$

where m_{H_2} is the mass of an individual hydrogen molecule and $f_{CO:H_2}$ is the abundance ratio of CO to H_2. Substitution shows that, if the CO in CRL 2688's fast wind is in LTE at 100 K, the CO:H_2 ratio is 5×10^{-4}, and the distance to CRL 2688 is 1 kpc, the total mass contributing to blueshifted line wing emission is $2.5 \times 10^{-3}\ M_\odot$, and the total mass contributing to redshifted line wing emission is $1.5 \times 10^{-3}\ M_\odot$. An additional $4 \times 10^{-3}\ M_\odot$ of fast wind material might emit at velocities confused with slow wind emission. If the blob model is an accurate description of the fast wind morphology, then each blob has a mass comparable to Jupiter's.

If the mass loss occurred predominantly in discrete episodes rather than in a continuous wind, estimating a mass-loss rate might not be very meaningful. However, a substantial fraction of the mass loss may have occurred in a continuous wind. The mass-loss rate of the fast wind is

$$\dot{M} = \frac{M_{fw}}{\tau} \approx \frac{M_{fw} v_{exp}}{R_{max}},$$

where τ is the time scale over which the mass was lost, and R_{max} is the maximum radius which the wind has attained. The most natural estimate for the age of the fast wind is about 400 yr, the approximate period CRL 2688 has been off the AGB. The average mass-loss rate for the fast wind is then $2 \times 10^{-5}\ M_\odot\ \mathrm{yr}^{-1}$. In 400 yr an unimpeded wind expanding at 50 km s^{-1} would have reached a radius of 6.3×10^{16} cm, corresponding to 4″ at 1 kpc. This is approximately the radius which we observe the fast wind to have obtained.

An interesting parameter for the winds of PPNs is the ratio of momentum in the wind to momentum in radiation from the central star,

$$\beta = \frac{\dot{M} v_{exp} c}{L_*}.$$

At a mass-loss rate of $2 \times 10^{-5}\ M_\odot\ \mathrm{yr}^{-1}$ and expansion velocity of 50 km s^{-1} the fast wind has $\beta = 2.5$, assuming a luminosity of $2 \times 10^4\ L_\odot$ (Ney et al. 1975). This compares to $\beta \approx 7.5$ for the slow wind.

Our estimate for the mass-loss rate of the fast wind is much lower than the mass-loss rate of $10^{-3}\ M_\odot\ \mathrm{yr}^{-1}$ estimated by Young et al. (1992) for their "high-velocity wind" (HVW) in CRL 2688. Our fast wind corresponds to their "medium-velocity wind" (MVW), for which they do not estimate a mass-loss rate. (According to Young et al. the CRL 2688 fast wind has two components, an HVW expanding at 100 km s^{-1} and a MVW expanding at 40–50 km s^{-1}.) If Young et al. had estimated a mass-loss rate for the MVW it probably would have been similar to or smaller than ours. Their very high estimate for the mass-loss rate of the HVW, which results in a β of 250, must be treated cautiously. These very large mass-loss rates are not required by the observational data, but are the result of model assumptions. Inspection of the above equations shows that

$$\dot{M} \propto \frac{T v_{exp}}{R_{max}}.$$

The temperature and maximum radial extent of the fast wind must be estimated in order to derive a mass-loss rate. Young et al., who did not resolve their HVW, assume $R_{max} = 5 \times 10^{15}$ cm, which corresponds to an angular radius of 0.″3 and an HVW lifetime of only 16 yr. Moreover Young et al. seem to assume a rather high temperature for their HVW. This is natural considering the small radius they suppose the HVW attains—the infrared core has a radius of 0.″5 and a temperature of about 200 K—but it has the effect of biasing the estimated mass-loss rate upward. A larger radial extent and lower temperature for the HVW would greatly reduce its estimated mass-loss rate. Within the constraints set by the available observational data, the HVW mass-loss rate could be as small as $10^{-5}\ M_\odot\ \mathrm{yr}^{-1}$.

4.5. *The Nucleosynthetic History of CRL 2688*

CRL 2688 shows evidence for CN-cycle processed material in its stellar wind. In the slow wind, ^{12}C:$^{13}C = 20$ (Wannier & Sahai 1987), while in the fast wind we find ^{12}C:$^{13}C = 5$. These rather low values place CRL 2688 among the J-type carbon stars, which have a considerably lower ^{12}C:^{13}C ratio than that of 40–80 found in most carbon stars (Lambert et al. 1986). The ^{12}C:^{13}C ratio of 5 in the fast wind is equal to the CN-cycle equilibrium value and indicates that envelope burning of carbon occurred. That the slow wind ratio is larger indicates that the stellar envelope was not fully mixed down to the CN-burning shell. The relatively low ^{16}O:^{17}O ratio, about 300, is consistent with (though it does not prove) NO-cycle processing to an extent consistent with equilibrium in the CN-cycle (Caughlan 1965).

If the fast wind material was heavily processed by the CN-cycle but incompletely processed by the slower NO-cycle, it is likely to be enriched in nitrogen and to have a lower C:O ratio than the slow wind. The possible enrichment of nitrogen in the fast wind is difficult to test observationally as long as the wind remains largely molecular, because the dominant nitrogen reservoir, N_2, is unobservable. However, the C:O ratio strongly affects the chemistry in the wind and should be observable. A decrease in the C:O ratio may be responsible for the lower HCN:CO abundance ratio we find in the fast wind. The HCN abundance is known to be quite sensitive to the C:O ratio. Observers have found that in oxygen-rich stars the HCN:H_2 ratio is typically about 3×10^{-7} (Lindqvist et al. 1988), while in carbon-rich stars the HCN:H_2 ratio is typically about 2×10^{-5} (Olofsson, Eriksson, & Gustafsson 1990). The HCN:H_2 ratio of 7×10^{-7} which we find for the fast wind is close to the usual value in oxygen-rich environments, while the estimates by other authors for the HCN:H_2 ratio in the slow

wind (e.g., NQRB) are closer to the value found in carbon-rich environments.

5. CONCLUSIONS

The submillimeter spectrum of CRL 2688 is rich, and even though the emission region is compact, it is bright in a number of lines. The high-velocity line wings first detected at millimeter wavelengths are much brighter in the submillimeter and can be observed in many molecular species.

We have observed velocity gradients similar to those found by BNQR. However, we do not believe these observed gradients prove that the envelope is rotating, because deviations from axial symmetry in the envelope could also cause the observed gradients, and we have indeed observed asymmetries in the fast wind which can account for the observed gradients. In particular, the fast wind seems to be extended and bipolar along both the N–S and E–W axes, contrary to the conventional description for the structure of bipolar nebulae. The morphology of the fast wind may be best accounted for by discrete mass-loss episodes involving the ejection of massive blobs, rather than continuous mass loss through a radiatively driven wind. Our submillimeter maps and spectra of the fast wind are strikingly similar to the H_2 $S(1)$ line maps and spectra of Smith et al. (1990), after accounting for differences of spatial and spectral resolution. However, if a continuous wind is responsible for the high-velocity line wings, its mass-loss rate is on the order of $2 \times 10^{-5}\ M_\odot\ \mathrm{yr}^{-1}$.

The envelope appears hotter in the submillimeter lines than was predicted by the model of TB90, derived by fitting millimeter wavelength lines observed at IRAM. This is due mainly to contamination of the submillimeter line profiles by emission from the warm, fast, wind material. However, the TB90 model is also unable to reproduce the observed line profiles from CRL 2688, probably because of the envelope's strong deviations from spherical symmetry, the uncertain contribution to the line profile of fast wind emission near line center, and variations with velocity in the absorption of fast wind emission by intervening slow wind material.

The fast wind has different elemental abundances, and perhaps a different chemistry, than the slow wind. The ^{12}C:^{13}C ratio is only 5 in the fast wind, compared to 20 in the slow wind. We interpret the difference as due to the different nucleosynthetic histories of the fast and slow wind material. The HCN:CO abundance ratio seems smaller in the fast wind than in the slow wind, although it is difficult to say by how much as the HCN abundance in the slow wind is uncertain.

We would like to thank the staff of the James Clerk Maxwell Telescope for their hospitality. The James Clerk Maxwell Telescope is operated by the Royal Observatory, Edinburgh, on behalf of the Science and Engineering Research Council of the United Kingdom, the Netherlands Organization for Scientific Research, and the National Research Council of Canada. P. A. J. would like to thank the Department of Astronomy of the University of Illinois, who were his very gracious hosts for an extended visit during which this paper was written. This work has been supported in part by the National Science Foundation under grants AST-8818327 and AST-9196077. P. A. J. was supported by a NASA Graduate Student Research Program fellowship during the period of this work. W. C. D. was supported in part by the L. W. Frohlich Research Fellowship of the NY Academy of Sciences.

REFERENCES

Aaquist, O. B., & Kwok, S. 1991, ApJ, 378, 599
Bieging, J. H., & Nguyen-Q-Rieu 1988, ApJ, 324, 516 (BNQR)
Bujarrabal, V., Gomez-Gonzalez, R., & Martin-Pintado, J. 1988, A&A, 204, 242 (BGBM)
Caughlan, G. R. 1965, ApJ, 141, 688
Cohen, M. 1981, PASP, 93, 288
Cohen, M., Dopita, M. A., Schwartz, R. D., & Tielens, A. G. G. M. 1985, ApJ, 297, 702
Cohen, M., & Kuhi, L. V. 1977, ApJ, 213, 79
Crampton, D., Cowley, A. P., & Humphreys, R. M. 1975, ApJ, 198, L135
Cummins, S. E., Linke, R. A., & Thaddeus, P. 1986, ApJS, 60, 819
Danchi, W. C., Gezari, D. Y., Degiacomi, C. G., Bester, M., Greenhill, L., & Townes, C. H. 1991, in preparation
Gammie, C. F., Knapp, G. R., Young, K., Phillips, T. G., & Falgarone, E. 1989, ApJ, 345, L87
Geballe, T. R., Tielens, A. G. G. M., Kwok, S., & Hrivnak, B. J. 1992, ApJ, 387, L89
Glassgold, A. E., Mamon, G. A., Omont, A., & Lucas, R. 1987, A&A, 180, 183
Greig, W. E. 1972, A&A, 18, 70
Heiligman, G. M., et al. 1986, ApJ, 308, 306
Hrivnak, B. J., & Kwok, S. 1991, ApJ, 368, 564
Icke, V., Balick, B., & Frank, A. 1992, A&A, 253, 224
Icke, V., Preston, H. L., & Balick, B. 1989, AJ, 97, 462
Jaminet, P. A., Danchi, W. C., Sutton, E. C., Russell, A. P. G. R., Sandell, G., Bieging, J. H., & Wilner, D. 1991, ApJ, 380, 461
Jaye, D., Tresch Fienberg, R., Fazio, G. G., Gezari, D. Y., Hoffmann, W. F., Lamb, G. M., Shu, P. K., & McCreight, C. R. 1989, AJ, 97, 809
Jewell, P. R., & Snyder, L. E. 1984, ApJ, 278, 176
Jura, M., & Kroto, H. 1990, ApJ, 351, 222
Kaler, J. B. 1983, ApJ, 271, 188
Kawabe, R., Ishiguro, M., Kasuga, T., Morita, K.-I., Ukita, N., Kobayashi, H., Okumura, S., Fomalont, E., & Kaifu, N. 1987, ApJ, 314, 322
Knapp, G. R. 1986, ApJ, 311, 731
Knapp, G. R., & Morris, M. 1985, ApJ, 292, 640
Kohoutek, L., & Surdej, J. 1980, A&A, 85, 161
Kwan, J., & Linke, R. A. 1982, ApJ, 254, 587
Lafon, J.-P. J., & Berruyer, N. 1991, A&A Review, 2, 249
Lambert, D. L., Gustafsson, B., Eriksson, K., & Hinkel, K. H. 1986, ApJS, 62, 373
Lindqvist, M., Nyman, L.-A., Olofsson, H., & Winnberg, A. 1988, A&A, 205, L15
Masson, C. R. 1990, ApJ, 348, 580
Morris, M. 1981, ApJ, 249, 572
Morris, M., Guilloteau, S., Lucas, R., & Omont, A. 1987, ApJ, 321, 888
Morris, M., & Reipurth, B. 1990, PASP, 102, 446
Ney, E. P., Merrill, K. M., Becklin, E. E., Neugebauer, G., & Wynn-Williams, C. G. 1975, ApJ, 198, L129
Nguyen-Q-Rieu, & Bieging, J. H. 1990, ApJ, 359, 131 (NQRB)
Nguyen-Q-Rieu, Winnberg, A., & Bujarrabal, V. 1986, A&A, 165, 204
Olofsson, H., Eriksson, K., & Gustafsson, B. 1990, A&A, 230, 405
Pauldrach, A., Puls, J., Kudritzki, R. P., Mendez, R. H., & Heap, S. R. 1988, A&A, 207, 123
Sahai, R. 1987, ApJ, 318, 809
———. 1990, ApJ, 362, 652
Sellgren, K., Luan, L., & Werner, M. W. 1990, ApJ, 359, 384
Smith, M. G., Geballe, T. R., Sandell, G., & Aspin, C. 1990, in Submillimeter Astronomy, ed. G. D. Watt & A. S. Webster (Dordrecht: Kluwer), 29
Sopka, R. J., Hildebrand, R., Jaffe, D. T., Gatley, I., Roellig, T., Werner, M., Jura, M., & Zuckerman, B. 1985, ApJ, 294, 242
Sopka, R. J., Olofsson, H., Johansson, L. E. B., Nguyen-Q-Rieu, & Zuckerman, B. 1989, A&A, 210, 78
Sutton, E. C., Danchi, W. C., Jaminet, P. A., & Ono, R. H. 1990, Int. J. Infrared Millimeter Waves, 11, 133
Trams, N. R., van der Veen, W. E. C. J., Waelkens, C., Waters, L. B. F. M., & Lamers, H. J. G. L. M. 1990, A&A, 233, 153
Truong-Bach, Morris, D., Nguyen-Q-Rieu, & Deguchi, S. 1990, A&A, 230, 431 (TB90)
van der Veen, W. E. C. J., Habing, H. J., & Geballe, R. R. 1989, A&A, 226, 108
Wannier, P. G., & Sahai, R. 1987, ApJ, 319, 367
Westbrook, W. E., Becklin, E. E., Merrill, K. M., Neugebauer, G., Schmift, M., Willner, S. P., & Wynn-Williams, C. G. 1975, ApJ, 202, 407
Young, K., Serabyn, E., Phillips, T. G., Knapp, G. R., Gusten, R., & Schulz, A. 1992, ApJ, 385, 265
Yusef-Zadeh, F., Morris, M., & White, R. L. 1984, ApJ, 278, 186
Zuckerman, B., & Aller, Lawrence H. 1986, ApJ, 301, 772